Nanorods of Well-Defined Length and Monodisperse Cross-Section Obtained from Electrostatic Complexation of Nanoparticles with a Semiflexible Biopolymer

Li Shi,[†,‡] Florent Carn,*[,†] François Boué,[‡] Gervaise Mosser,[§] and Eric Buhler*[,†,‡]

[†]Laboratoire Matière et Systèmes Complexes (MSC), UMR 7057, Université Paris Diderot-Paris 7, Bâtiment Condorcet, 75205 Paris cedex 13, France

[‡]Laboratoire Léon Brillouin, UMR 12 CEA-CNRS, CEA Saclay, 91191 Gif-sur-Yvette, France

[§]Laboratoire Chimie de la Matière Condensée de Paris, UMR 7574, UPMC, Collège de France, 11 place Marcelin Berthelot, 75005 Paris, France

ABSTRACT: We show by combining small-angle X-ray scattering (SAXS) and cryo-transmission electron microscopy (cryo-TEM) that anionic silica nanoparticles (SiNPs) assemble into well-defined 1D cluster when mixed with a dilute solution of semiflexible chitosan polycation. The nanorods are stable in excess of SiNPs and composed of 10 SiNPs well-ordered into straight single strands with length $L_{rod} \approx 184.0$ nm and radius $R_{rod} = 9.2$ nm $= R_{SiNPs}$. We point out that the ratio between the chitosan persistence length and the SiNP radius, which is here equal to 1, can be the determining condition to obtain such original objects.
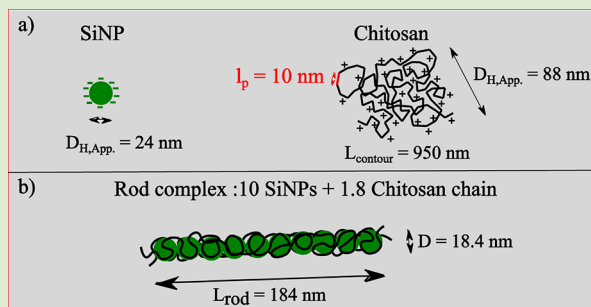
A wide range of technological applications on nanometric rods has appeared in the last 10 years, but a severe restriction is the complexity of most syntheses. We present here a surprisingly simple, cheap, and environmentally friendly approach based on an abundant natural polymer and spherical nanoparticles (NPs). Nanometric rods open routes toward new applications such as a plasmon-based waveguide, biosensors, nanorulers, or theragnostic materials.[1] Of course, they critically depend on the controlled ordering of the nanobuilding block that determines their collective interactions.[2] Opposite to elaborated procedures, such as rodlike nanocrystals syntheses or well-controlled 1D structures built on a surface, is the more basic approach of 1D assembly of preformed spherical nanoparticles, now largely available. This can be template- or nontemplate-assisted assembly.[3] In the first case, rigid polymers,[4] viruses, or carbon nanotubes[5] have served as a template to assemble NPs.[1b,c,j,k,4−8] In the second case, the anisotropic or isotropic functionalization of nanoparticles by electrolytes, surfactants, or biomolecular ligands has already enabled the directional assembly of nanoparticles.[1e,f,9−13] Still the problem, generally, is the involvement of multistep protocols that necessitate sophisticated chemical and/or physical methods. Moreover, this complexity combines with the one of a "shape diagram", since these processes can also lead to either extended ramified chains or very small entities (dimers or trimers) instead of rods with a finite and intermediate size.[9]

Our simple alternative is based on electrostatic complexation between well-known spherical inorganic nanoparticles and an abundant natural semiflexible polyelectrolyte of opposite charge. Electrostatic associations, which can lead to solid–liquid or liquid–liquid phase separation, have attracted considerable theoretical and experimental attention in the last two decades. A great variety of nanostructured complexes has been reported, but to the best of our knowledge, significant control over morphology is scarcely claimed, apart from the preparation of isotropic shapes or necklace-like aggregates—a few of them being characterized in great detail.[14,15] Although post-treatments for stretching preformed physical complexes into highly ordered 1D assembly have been reported,[16] to date one-pot preparations of nanometric rod shaped complexes are almost nonexistent.

Using this electrostatic complexation approach, after simple mixing of model silica NPs (SiNPs) and cationic chitosan chain solutions, we obtain for the first time a stable dispersion of well-defined nanometric rods composed of individual NPs in close contact. The evidencing technique is small angle X-ray scattering (SAXS), which enables us to estimate the characteristic sizes and the local structural parameters of the rods: (i) the number of NPs (10 in average) and chitosan chains (1−2) per rod; (ii) the rod length (≈ 200 nm) and its axial radius R_{rod}, equal to the radius of the SiNPs ($R_{SiNP} \approx 10$ nm). It is interesting to compare the NP radius with the polymer chain intrinsic persistence length $L_p \approx 7.5$ nm.[17] We see that $L_p/R_{SiNP} \approx 1$ and can then propose a mechanism of formation, where chitosan chains wrap around the particles. To compare to an

illustrious case, let us note that this is in striking contrast with DNA packaging into chromatin, where an almost rigid polymer with larger persistence length $L_p \approx 50$ nm is compacted around small oppositely charged histone with $R \approx 3.5$ nm. As a complementary technique, in real space, we used cryogenic transmission electronic microscopy (cryo-TEM); combined with SAXS this gives a wide range of observation scale from the nanometer to the micrometer scale.

First the two genuine components had to be carefully characterized. The stock solutions of chitosan or SiNPs suspensions were previously prepared (at twice the final concentration before mixing) in water buffer with C_{CH_3COOH} = 0.3 M and C_{CH_3COONa} = 0.2 M. Both partners are charged: about SiNPS, in these conditions, we have roughly estimated from the electrophoretic mobility ($\mu = -2.3 \times 10^{-8}$ m²·V⁻¹·s⁻¹) that each SiNP displays 25 elementary negative charges via the Hückel equation (it corresponds to a surface charge density of 0.02 charges·nm⁻²). The autocorrelation function of concentration fluctuations, $g^{(1)}(q,t)$, measured by dynamic light scattering (DLS), decreases monoexponentially with a characteristic relaxation time inversely proportional to q^2 and leads to $R_{H,SiNP}$ = 12 nm. About chitosan, we briefly recall that it is a linear cationic polysaccharide derived by alkaline deacetylation of chitin (found in crustacean shells) and is constituted of two residues linked by β-(1→4) glycosidic bonds, N-acetyl glucosamine and glucosamine (deacetylated fraction measured by NMR, f_D = 87.5%),[17] which is charged. In the preparation conditions, it exhibits a high polyelectrolyte character with approximately one positive charge per segment (of size 5 Å). The polydispersity index of chitosan is 1.3 and was determined using gel permeation chromatography (GPC) experiments.[17] The weight-average molecular weight of chains, M_W = 313 K ($\approx$ 2000 segments), and the radius of gyration, R_G = 66 nm, were deduced from static light scattering (SLS) measurements and a classical Guinier analysis, and $R_{H,chitosan}$ = 44 nm (hydrodynamic radius) from DLS. Thus in the dilute range of chitosan concentration ($C_{chitosan}$ = 0.1 g·L⁻¹), chitosan chains are in the typical semirigid polymer-like conformation with $R_G/R_H = 66/44 \approx 1.5$. In summary, both chitosan chains and SiNPs are well-dispersed and stable in solution.

The buffer solution is the aqueous solution consisting of a mixture of 0.3 M CH_3COOH and 0.2 M CH_3COONa. Since SiNPs and chitosan chains are both fully charged in a relatively small pH range, this buffer was used as a mean of keeping the pH at a constant value of 4.5 in the whole range of mixing ratio. Within these experimental conditions the electrostatic complexation between the two partners takes place readily.

Figure 1 illustrates the macroscopic phase behavior of the mixtures determined by visual inspection at 20 °C for the molar ratio, $r = C_{chitosan}/C_{SiNPs}$, comprised between r = 8.6 and r = 0.0013 with constant $C_{chitosan}$ = 0.01 g·L⁻¹. The samples are obtained after continuous stirring for several hours and let aging for 2 weeks in static conditions; two phase boundaries are detected at r^* = 1.88 ± 0.20 and r^{**} = 0.030 ± 0.005. In domains I and III of the phase diagram, obtained for $r < r^*$ and $r > r^{**}$, respectively, stable transparent single phase samples were observed. In the intermediate domain no. II, turbid samples progressively evolve under aging toward macroscopically biphasic samples; both the supernatant and the dense lower phase display a liquid character according to qualitative flowing tests. Besides, it was also found that the phase boundaries of the system vary with either pH or ionic strength.
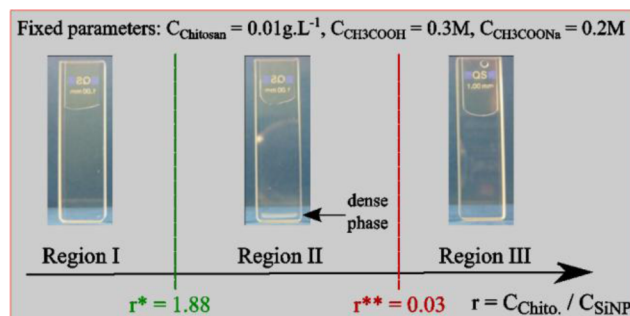

Figure 1. Schematic phase diagram of chitosan/SiNP mixtures at $C_{chitosan}$ = 0.01 g·L⁻¹. Along the horizontal axis are reported the different concentration thresholds (r^* (region I/II) and r^{**} (region II/III)) observed in the presence of C_{CH_3COOH} = 0.3 M and C_{CH_3COONa} = 0.2 M at 20 °C.

This kind of liquid−liquid phase separations have often been observed in mixed systems involving polyelectrolytes and oppositely charged colloids and were generally discussed in the frame of associative phase separation or complex coacervation processes.[14,15] In the buffer at pH = 4.5, the mechanism of complexation, that is of electrostatic origin, is the same in the whole range of mixing ratio. In the frame of this letter, we propose a thorough structural study of the soluble complexes obtained in monophasic domain no. III.

SAXS experiments were carried out at T = 20 °C on the instrument ID-02 (ESRF, Grenoble) with configurations allowing a large q range varying between 0.0011 Å⁻¹ and 0.57 Å⁻¹. The final spectra are given in absolute units of cross-section (cm⁻¹) following standard procedures.[18] For the individual SiNPs, Figure 2a (lower curve) shows, in agreement with light scattering, that NPs are dispersed individually. As detailed in the Experimental Section, the form factor oscillations, damped by a size distribution, are well-reproduced with $I(q)$ calculated as indicated in the Experimental Section. The SiNPs solution is well-represented by a suspension of hard spheres with R = 9.2 nm and a variance σ = 0.12. Extrapolation of the scattered intensity to the zero-wave vector, $I(0)$, gives the weight-average molecular weight, $M_{W,SiNP} = 3 \times 10^6$ g·mol⁻¹.

For complexes (upper curve), due to the high electronic density and concentration of the SiNPs, the signal is dominated by the scattering of the SiNPs (whether they belong or not to complexes). Due to the small concentration and molecular weight of chitosan chains their signal is negligible. The scattering curve exhibits the overall behavior characterized by the following sequence: a Guinier regime in the low q range associated with the finite size and mass of the scattered objects, one intermediate regime in which the q dependence is described by a power law with an exponent close to −1, a second Guinier regime at higher q corresponding to the cross-section of the assemblies, and finally well-defined oscillations associated to the shape-dependent form factor of the particle cross-section.

For the data lying in intermediate and low-q Guinier regimes, one can use the Fisher−Burford expression[19] that is well-suited to study fractal colloidal aggregates:

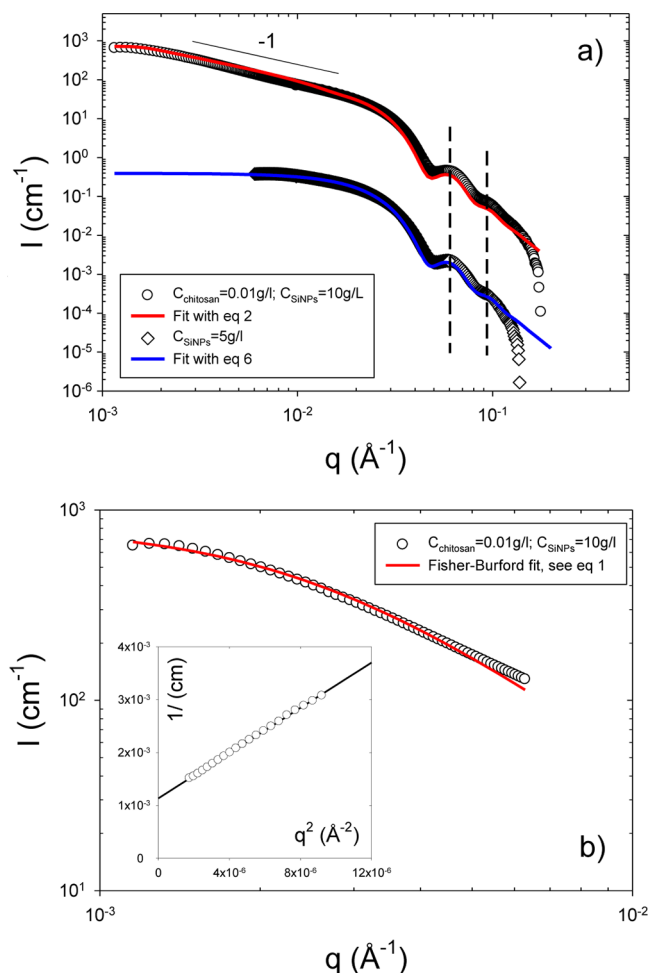$$I(q) = I(0) \frac{1}{\left(1 + \frac{2}{3D_f} q^2 R_G^2\right)^{D_f/2}}$$

(1)

Figure 2. (a) SAXS spectra from a $C_{chitosan} = 0.01$ g·L^{-1}/$C_{SiNP} = 10$ g·L^{-1} solution (upper curve, $r = 0.01$) and a $C_{SiNP} = 5$ g·L^{-1} solution (lower curve) with $C_{CH_3COOH} = 0.3$ M and $C_{CH_3COONa} = 0.2$ M. For clarity the curves have been shifted by two log units along the y-axis with respect to each other. The continuous lines represent the fits of the data. (b) Low-q scattering curves in a log–log representation. The solid line represents the Fisher–Burford fit with $D_f = 1$, whereas the inset represents $I(q)^{-1}$ versus q^2 and the best linear fit.

where D_f represents the exponent of the power law in the intermediate regime. The fit of the above expression to the scattering curve is shown in Figure 2b, imposing for D_f the value of 1 characteristic of rigid rod. At low qR_G eq 1 is equivalent to the well-known Guinier expression, and the fit provides a value of the radius of gyration, R_G, and of the zero-wave vector scattered intensity, $I(0)$, in good agreement with the initial slope of the curve $I^{-1} = f(q^2)$ shown in the inset. We obtain $R_G = 77 \pm 8$ nm and $M_W = (31 \pm 3) \times 10^6$ g·mol^{-1}, the different values within the uncertainty depending on the method.

Knowing now D_f, we propose to model the scattering of the NPs self-assemblies over the whole q range by the form factor of fractal objects with the following expression:[20]

$$\frac{I(q)}{(\Delta\rho)^2\phi} = VP(q)$$

$$= N_{agg}q^{-D_f}\frac{\int_0^\infty P_{Spheres}(q, R)L(R, \sigma)R^3\mathrm{d}R}{\int_0^\infty L(R, \sigma)R^3\mathrm{d}R} \quad (2)$$

where N_{agg} is the number of silica nanoparticles inside the complexes, D_f is the fractal dimension of the aggregates, and $P(q)_{spheres}$ is the sphere form factor (see eq 7 in the Experimental Section). We assume the structure factor between aggregates to be close to 1. From the fit of Figure 2a (upper curve), we obtain $R = 9.2$ nm, $\sigma = 0.12$, $D_f = 1$, and $N_{agg} = 10$. These results call for two conclusions. First, SiNPs self-assemble in a well-ordered 1D geometry. Second, the overall nanoobjects are single strands with no lateral associations, as shown by the cross-section radius and polydispersity values that are similar to those of free SiNPs. Similar SAXS results were obtained in the whole range of molar ratio in domain III ($r = 0.01$, 0.007, and 0.004).

Cryo-TEM was used to confirm the detailed structure of the soluble complexes in the direct space. Figure 3a shows a

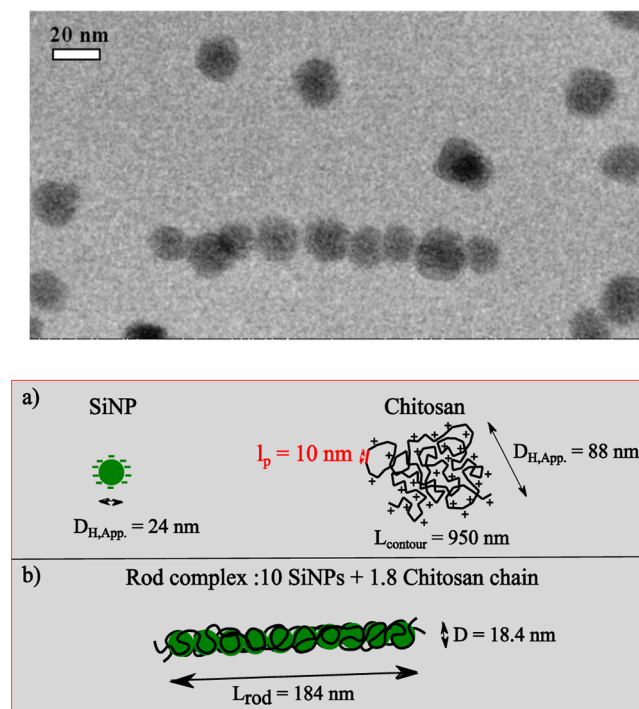**Figure 3.** (a) Cryo-TEM image of $C_{chitosan} = 0.01$ g·L^{-1}/$C_{SiNP} = 10$ g·L^{-1} solutions with $C_{CH_3COOH} = 0.3$ M and $C_{CH_3COONa} = 0.2$ M ($r = 0.01$). (b) Schematic diagram depicting the nanorod characteristic lengths.

representative TEM image of the chitosan−SiNP complexes surrounded by individual nanoparticles. It appears that all complexes consist of 1D array of SiNPs in contact with each other inside the complexes. According to the analysis of a large number of images (around 50), the nanometric rods are single strands with average characteristics such as: $\langle N_{agg,Cryo}\rangle \approx 9$ and $\langle L_{agg,Cryo}\rangle = 166$ nm. Since the radius of the rod section appears constant in the pictures and branched structures are not observed, we conclude that nanorods correspond to single strands of NPs, rather rigidly. These observations agree with SAXS analysis giving $L_{rod} = 2R \times N_{agg} = 184$ nm, as an average over the whole sample, in situ in the solution on representative volume (cm^3) (see Figure 3b).

Unfortunately the low electronic contrast between the biopolymer and the surrounding medium, grid membrane for TEM or water for SAXS, does not enable us to clearly identify the number of chain per complex and their arrangement in the

nanorod structure. However SAXS sheds some light on this aspect, by allowing us to estimate the amount per complexes of silica, and more indirectly of chitosan. A simple calculation has been made on the basis of the average number of individual nanoparticles and of nanorods determined by fitting the scattering pattern by the following equation:

$$I(q) = \phi_{\text{rods}}I_{\text{rods}}(q) + \phi_{\text{indiv NPs}}I_{\text{indiv NPs}}(q) \qquad (3)$$

where $I_{\text{rods}}(q)$ and $I_{\text{indivNPs}}(q)$ are the scattered intensities related respectively to the form factor of the rods and of the individual spherical SiNPs. The best agreement with the data of Figure 2a is obtained for $\phi_{\text{indivNPs}} = 4.3 \times 10^{-3}$ and $\phi_{\text{rods}} = 2.3 \times 10^{-4}$, and for a number of silica particles inside the nanorods slightly larger, $N_{\text{agg}} = 14$. Then, considering that SiNPs are in excess and that, according to cryo-TEM, only SiNPs present in complexes display the ribbed texture attributed to chitosan chain binding, one can hypothesize that all of the chitosan chains are involved in the complexes. Finally, one derives an average concentration of 1.8 chains of chitosan per nanorod. This result first shows that very few chains are needed to allow SiNPs organization into nanorods. A second striking point is that the contour length of the biopolymers ($\approx$ 943 nm in weight average) is significantly higher than the average nanorod length ($\approx$ 184 nm) suggesting that chitosan chains are somehow wrapped around SiNPs. This wrapping could occur owing to the adequation between the chitosan chain flexibility and the NP surface curvature. This is driven by the persistence length, and a simple calculation shows that approximately 8−10 chitosan persistence lengths ($L_{\text{p}} \approx 7.5$ nm) are necessary to make a complete turn around a NP ($2\pi R$), suggesting that the chain wrapping around the 10−14 SiNPs into a nanorod is somehow helical ($10 \times L_{\text{p}} \times N_{\text{agg}} \approx 2\pi R \times N_{\text{agg}} \approx L_{\text{chitosan}}$). This may explain the single strand rodlike structure and shows that the chitosan mass could directly determine the nanorod length.

The nanorod length gives a lower bound for the nanorod persistence length: $L_{\text{p,rod,min}} = L_{\text{rod}} = 184$ nm. The persistence length can also be expressed using the bending stiffness B_{s} and the Young modulus E knowing the section of the rod: $B_{\text{s}} = E \times I$. In the case of a rigid and uniform rod, I can be expressed as $I = \pi R^4/4$ (where R is the radius).[21] A lower bound for the modulus of such nanorods can then be estimated: $E_{\text{min}} = (L_{\text{p,rod,min}} \times kT \times 4)/(\pi R^4) = 1.32 \times 10^5$ Pa.

In conclusion, we have demonstrated by combining SAXS and cryo-TEM that well-defined nanorod complexes, quasi-monodisperse in radius, can be obtained by simply mixing cationic chains of natural chitosan with an excess of anionic SiNPs. These 1D aggregates are stable, single-strand, and composed in average of 10 SiNPs for 1.8 chitosan chains. The mechanism of these nanorods formation is striking since, to the best of our knowledge, this is the first time that such kind of nanorods are prepared with a semiflexible polyelectrolyte displaying a persistence length as low as $\approx$8 nm. We point out that the ratio between chitosan persistence length and SiNPs radius, L_{p}/R, which is here close to 1, may be a determining condition to obtain such objects. Experiments are under course to further clarify the global mechanism of these nanorods formation. In the future, we hope that the identification of this parameter L_{p}/R (as well as the mixing ratio) will open the way toward the control clustering of individual nanoparticles into complexes with a tailored shape.

■ EXPERIMENTAL SECTION

The SAXS experiments were performed at the European Synchrotron Radiation Fability (ESRF; Grenoble, France) on the ID-02 instrument using the pinhole camera at the energy of 12.46 keV at two sample-to-detector distances (1 m and 8 m) corresponding to a q-range varying between 0.0011 Å^{-1} and 0.57 Å^{-1}. The absolute units are obtained by normalization with respect to water (high q-range) or lupolen (low q-range) standard. The total scattered intensity, $I(q)$, of colloidal objects—neglecting the chitosan chains signal—can be expressed by the following equation:

$$I(q) = \phi(\Delta\rho)^2 VP(q)S(q) \qquad (4)$$

where $q = 4\pi/\lambda \times \sin\theta/2$ is the wave vector, ϕ is the volume fraction, $(\Delta\rho)^2 = (\rho - \rho_{\text{solvent}})^2$ the contrast term, V the volume of the scattered objects (related to the weight-average molecular weight M_{W} of the objects), $P(q)$ the form factor, and $S(q)$ the structure factor. In the first approximation we will consider that interobject interactions are negligible (diluted regime) and that cross-terms and virial effects are neglected in our fitting procedure (analysis realized in a q-range where $I(q) \approx P(q)$). For SAXS, the scattering length densities (SLDs) are defined by $\rho = 1/(mv \times 1.66 \times 10^{-24}) \times r_{\text{el}} \times \sum n_i Z_i$, where $r_{\text{el}} = 0.28 \times 10^{-5}$ nm is the electron radius, Z_i the atomic number of element i, m the monomer mass, and v the monomer specific volume (0.478 cm$^3 \cdot$g^{-1} for chitosan and 0.4545 cm$^3 \cdot$g^{-1} for silica). For chitosan and SiNPs we found $\rho_{\text{chitosan}} = 18.7 \times 10^{10}$ cm^{-2} and $\rho_{\text{SiNP}} = 18.5 \times 10^{10}$ cm^{-2}, respectively.

We first characterized the scattering from a SiNPs suspension, introducing a polydispersity in size of the scattered objects described by a log-normal distribution, $L(r, R, \sigma)$, where r is the radius, R the mean radius, and σ the variance:

$$L(r, R, \sigma) = \frac{1}{r\sigma\sqrt{2\pi}}\exp\left(-\frac{1}{2\sigma^2}\ln^2\left(\frac{r}{R}\right)\right) \qquad (5)$$

Thus, neglecting the virial effects (assuming $S(q) = 1$) at low concentration in the presence of salt, it is classical to define the global scattering intensity by the following relation:

$$I(q) = \phi(\Delta\rho)^2 V \int_0^{\infty} P(q, r)L(r, R, \sigma)\mathrm{d}r \qquad (6)$$

Figure 2a shows the scattering of the pure SiNPs solution (lower curve), which can be fitted satisfactorily by means of the form factor expression derived for hard spheres of radius R:

$$P(q) = 9 \times \left[\frac{\sin(qR) - qR\cos(qR)}{(qR)^3}\right]^2 \qquad (7)$$

The form factor oscillations, damped by the size distribution, are well-reproduced with $I(q)$ calculated as indicated above (eqs 6 and 7). The SiNPs solution is well-represented by a suspension of hard spheres with $R = 9.2$ nm and $\sigma = 0.12$. Extrapolation of the scattered intensity to zero-wave vector, $I(0)$, gives the weight-average molecular weight, $M_{\text{W,SiNP}} = 3 \times 10^6$ g·mol^{-1}.

The discussion of the signal from the complexes is given in the main text.

Cryo-transmission electron microscopy (cryo-TEM) was performed on vitrified complexes prepared at $r = 0.01$. In brief, a drop of the solution to be imaged was poured onto a TEM carbon grid covered by a 100 nm thick polymer perforated membrane. The drop was blotted with filter paper, and the grid was quenched rapidly in liquid ethane to avoid the crystallization of the aqueous phase. The vitrified samples were then stored under liquid nitrogen and transferred to the vacuum column of a Tecnai TEM microscope operating at 120 kV. The magnification for the cryo-TEM experiments was selected at 40 000×.

■ AUTHOR INFORMATION

Corresponding Author
*E-mail: eric.buhler@univ-paris-diderot.fr and florent.carn@univ-paris-diderot.fr.

■ REFERENCES

(1) For instance: (a) Han, M.; Gao, X.; Su, J. Z.; Nie, S. *Nat. Biotechnol.* **2001**, *19*, 631. (b) Li, L.-S.; Stupp, S. I. *Angew. Chem., Int. Ed.* **2005**, *44*, 1833. (c) Chen, Y.; Liu, H.; Ye, T.; Kim, J.; Mao, C. *J. Am. Chem. Soc.* **2007**, *129*, 8696. (d) Frankamp, B. L.; Boal, A. K.; Rotello, V. M. *J. Am. Chem. Soc.* **2002**, *124*, 15146. (e) Sardar, R.; Shumaker-Parry, J. S. *Nano Lett.* **2008**, *8*, 731. (f) DeVries, G. A.; Brunnbauer, M.; Hu, Y.; Jackson, A. M.; Long, B.; Neltner, B. T.; Uzun, O.; Wunsch, B. H.; Stellacci, F. *Science* **2007**, *315*, 358. (g) Maier, S. A.; Kik, P. G.; Atwater, H. A.; Meltzer, S.; Harel, E.; Koel, B. E.; Requicha, A. A. G. *Nat. Mater.* **2003**, *2*, 229. (h) Maier, S. A.; Brongersma, M. L.; Kik, P. G.; Meltzer, S.; Requicha, A. A. G.; Atwater, H. A. *Adv. Mater.* **2001**, *13*, 1501. (i) Nomura, W.; Ohtsu, M.; Yatsui, T. *Appl. Phys. Lett.* **2005**, *86*, 181108. (j) Wang, C.-J.; Huang, L.; Parviz, B. A.; Lin, L. Y. *Nano Lett.* **2006**, *6*, 2549. (k) Yatsui, T.; Ryu, Y.; Morishima, T.; Nomura, W.; Kawazoe, T.; Yonezouva, T.; Washizu, M.; Fujita, H.; Ohtsu, M. *Appl. Phys. Lett.* **2010**, *96*, 133106. (l) Anker, J. N.; Paige Hall, W.; Lyandres, O.; Shah, N. C.; Zhao, J.; Van Duyne, R. P. *Nat. Mater.* **2008**, *7*, 442. (m) Shenhar, R.; Norsten, T. B.; Rotello, V. M. *Adv. Mater.* **2005**, *17*, 657. (n) Wyrwa, D.; Beyer, N.; Schmid, G. *Nano Lett.* **2002**, *2*, 419.

(2) (a) Nie, Z.; Petukhova, A.; Kumacheva, E. *Nat. Nanotechnol.* **2010**, *5*, 15. (b) Halas, N. J.; Lal, S.; Chang, W.-S.; Link, S.; Nordlander, P. *Chem. Rev.* **2011**, *111*, 3913.

(3) (a) Rycenga, M.; Cobley, C. M.; Zeng, J.; Li, W.; Moran, C. H.; Zhang, Q.; Qin, D.; Xia, Y. *Chem. Rev.* **2011**, *111*, 3669. (b) Jones, M. R.; Osberg, K. D.; Macfarlane, R. J.; Langille, M. R.; Mirkin, C. A. *Chem. Rev.* **2011**, *111*, 3736. (c) Sacanna, S.; Pine, D. J. *Curr. Opin. Colloid Interface Sci.* **2011**, *16*, 96. (d) Sacanna, S.; Irvine, W. T. M.; Chaikin, P. M.; Pine, D. J. *Nature* **2010**, *464*, 575.

(4) Haeshin Lee, Y. L.; Messersmith, P. B.; Park, T. G. *Macromol. Rapid Commun.* **2010**, *31*, 2109.

(5) Ou, Y.-Y.; Huang, M. H. *J. Phys. Chem. B* **2006**, *110*, 2031.

(6) Hsieh, S.; Hsieh, C. W. *Chem. Commun.* **2010**, *46*, 7355.

(7) Lin, J.; Wenchong, W.; Harold, F. *Small* **2009**, *5*, 2819.

(8) Bhattacharya, R.; Ranjan Patra, C.; Wang, S.; Lu, L.; Yaszemski, M. J.; Mukhopadhyay, D.; Mukherjee, P. *Adv. Funct. Mater.* **2006**, *16*, 395.

(9) Hofmann, A.; Schmiel, P.; Stein, B.; Graf, C. *Langmuir* **2011**, *27*, 15165.

(10) Lattuada, M.; Hatton, T. A. *NanoToday* **2011**, *6*, 286.

(11) Peiris, P. M.; Schmidt, E.; Calabrese, M.; Karathanasis, E. *PLoS One* **2011**, *6*, e15927.

(12) Hussain, I.; Brust, M.; Barauskas, J.; Cooper, A. I. *Langmuir* **2009**, *25*, 1934.

(13) Chen, C.-L.; Rosi, N. L. *J. Am. Chem. Soc.* **2010**, *132*, 6902.

(14) (a) Gummel, J.; Cousin, F.; Boué, F. *J. Am. Chem. Soc.* **2007**, *129*, 5806. (b) Kizilay, E.; Kayitmazer, A. B.; Dubin, P. L. *Adv. Colloid Interface Sci.* **2011**, *167*, 24−37.

(15) Morfin, I.; Buhler, E.; Cousin, F.; Grillo, I.; Boué, F. *Biomacromolecules* **2011**, *12*, 859.

(16) Nakao, H.; Shiigi, H.; Yamamoto, Y.; Tokonami, S.; Nagaoka, T.; Sugiyama, S.; Ohtani, T. *Nano Lett.* **2003**, *3*, 1391.

(17) (a) Buhler, E.; Guetta, O.; Rinaudo, M. *Int. J. Polym. Anal. Character.* **2000**, *6*, 155. (b) Buhler, E.; Rinaudo, M. *Macromolecules* **2000**, *33*, 2098.

(18) Jouault, N.; Nguyen, R.; Rawiso, M.; Giuseppone, N.; Buhler, E. *Soft Matter* **2011**, *7*, 4787.

(19) (a) Fisher, M. E.; Burford, R. J. *Phys. Rev.* **1967**, *156*, 583. (b) Dietler, G.; Aubert, C.; Cannell, D. S.; Wiltzius, P. *Phys. Rev. Lett.* **1986**, *57*, 3117.

(20) Rivière, C.; Wilhelm, C.; Cousin, F.; Dupuis, V.; Gazeau, F.; Perzinski, R. *Eur. Phys. J. E* **2007**, *22*, 1.

(21) Bloom, K. S. *Chromosoma* **2008**, *117*, 103.